ACS Biomaterials SCIENCE & ENGINEERING

pubs.acs.org/journal/abseba

Article

Developing [60]Fullerene Nanomaterials for Better Photodynamic Treatment of Non-Melanoma Skin Cancers

Maciej Serda,* Grzegorz Szewczyk, Olga Krzysztyńska-Kuleta, Julia Korzuch, Mateusz Dulski, Robert Musioł, and Tadeusz Sarna

Cite This: *ACS Biomater. Sci. Eng.* 2020, 6, 5930−5940

Read Online

ACCESS | Metrics & More | Article Recommendations | Supporting Information

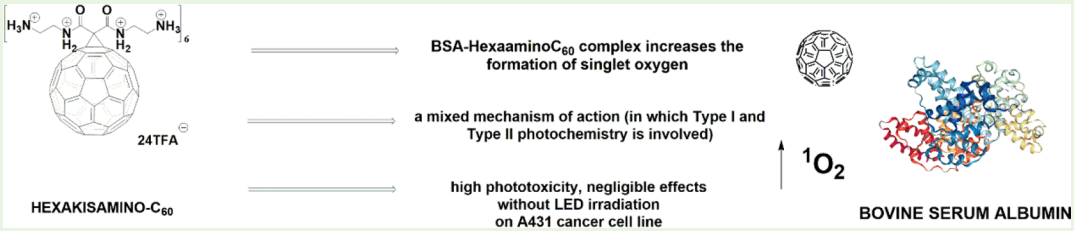

ABSTRACT: Skin cancer is the most common cancer in the U.S.A. and Europe. Its subtype, squamous skin carcinoma (SCC), if allowed to grow, has the potential to metastasize and can become deadly. Currently, carbon nanomaterials are being developed to treat cancer due to their attractive physicochemical and biological properties such as an enhanced permeability effect and their ability to produce reactive oxygen species. Here, we describe the synthesis of two water-soluble aminofullerenes (MonoaminoC_{60} and HexakisaminoC_{60}), which were evaluated as novel [60]fullerene based photosentizers exhibiting anticancer properties. Moreover, the previously described neutral glycofullerene GF1 and its peracetylated lipophilic precursor MMS48 were compared with the aminofullerenes for their ability to generate reactive oxygen species and oxidize lipids. Remarkably, the generation of singlet oxygen and a superoxide radical by HexakisaminoC_{60} was found to be markedly elevated in the presence of bovine serum albumin and NADH, respectively. Mechanistic studies of lipid peroxidation using cholesterol as a unique reporter molecule revealed that although all four fullerene nanomaterials primarily generated singlet oxygen, superoxide anion was also formed, which suggest a mixed mechanism of action (in which Type I and Type II photochemistry is involved). The [60]fullerene derivative HexakisaminoC_{60} was also studied for its phototoxicity in squamous skin cancer cell line (A431) using the MTT test and propidium iodide staining.

KEYWORDS: *[60]fullerene, non-melanoma skin cancer, photodynamic therapy, singlet oxygen, EPR spin trapping, lipid peroxidation*

INTRODUCTION

Non-melanoma skin cancer (NMSC) is a serious malignant disease, which frequently occurs in older Caucasian patients and is categorized into two subgroups: basal cell carcinoma (BCC) and squamous cell carcinoma (SCC).[1,2] While metastatic BCC is rarely diagnosed,[3,4] metastatic SCC is characterized by a specific proliferation of invasive squamous cells and has an annual incidence of approximately 4%. Despite its statistically low mortality, this malignancy causes considerable problems in the healthcare systems in Europe, the U.S.A., and Australia. A plethora of risk factors are involved in melanoma and NMSC pathogenesis including UV and ionizing radiation, and the occurrence of alterations in the oncogenes/tumor suppressor genes such as BRAF, PTEN, and TP53.[5] The metastatic potential, mortality rates, and reoccurrence are higher for SCC than for BSC, and the current clinical treatment options include surgical excision, radiation therapy, chemotherapy, and any combination of the above.[6] Photodynamic therapy has been used as a successful treatment method in clinical practice with the topical use of 5-aminolevulinic acid methyl ester (MAL-PDT) in patients suffering from basal cell carcinoma.[7] Some novel chemotherapeutic strategies are also under development for the treatment of skin cancer including the use of the inhibitors of the protein tyrosine kinases such as EGFR and non-receptor Src kinases.[8,9]

The use of nanomedical approaches has been extensively explored for both diagnosing and treating skin cancers, including EGFR-targeted immunoliposomes, 5-ALA nanoconjugates with polylactic acid and engineered gold nanoparticles.[10−12] Engineered carbon nanomaterials are promising new approaches, mainly for their cancer photodynamic therapy (PDT) and antimicrobial photodynamic inactivation (PDI) applications.[13,14] The water-soluble fullerene derivatives tend

Received: June 23, 2020
Accepted: September 3, 2020
Published: September 3, 2020

https://dx.doi.org/10.1021/acsbiomaterials.0c00932
ACS Biomater. Sci. Eng. 2020, 6, 5930−5940

to be great candidates for photosensitizers because of the high triplet yields and the long triplet lifetime of the C_{60} cage, which facilitate their interaction with molecular oxygen.[15] The pioneering studies performed by the Hamblin and Wilson groups, which were mainly focused on the Bingel–Hirsch monoadducts and functionalized pyrrolidinofullerenes, demonstrated the utility of water-soluble aminofullerenes in PDT.[16−19] An interesting addition to the traditional C_{60}-based photosensitizers are the Gadolinium-containing endohedral fullerenes and the derivatives of $Gd@C_{82}$, which are also used as MRI-contrast agents and to stimulate immunological responses followed by modulating the tumor microenvironment.[20,21] Despite weak absorption of [60]fullerenes in the deep-penetrating NIR region of the spectrum (above 700 nm), they are able to perform the *Type 1* and *Type 2* photochemical reactions and are highly resistant to photobleaching, which make them an attractive option as photosensitizers for most PDT applications.[17] Application of low-penetrating blue light illuminations can be overcome by using femtosecond lasers in two-photon excitation experiments or upconverting nanoparticles such as $NaYF_4$ with Yb^{3+}/ Er^{3+} dopants *via* covalent conjugation/coating absorption to the photosensitizer scaffold.[22]

Previous studies, performed by our group, demonstrated that the water-soluble glycofullerenes were photoactive and they localized inside the nuclear envelope of the pancreatic stellate cells (PSCs).[23] Moreover, the results that were obtained from the cited studies revealed that glycofullerenes could effectively inhibit the nonreceptor tyrosine kinases, with a selectivity toward the FYN A protein, which is an important potential target for skin cancers, even in the presence of the FBS proteins.[24] This observation could be of use in combinational therapies because tyrosine kinase inhibitors are also being investigated in the treatment of skin cancers.[25] At the same time, several reports have demonstrated interactions between the albumin proteins and the photosensitizers, which played an important role in their biodistribution within the tumor tissues.[26] The water-soluble fullerenes are well-known for their interactions with human serum albumin, which forms a stable complex with the [60]fullerene *tris*-malonic acid (C_3 isomer called CF)[27] or PCBM fullerene.[28] Interestingly, although no effects on the quantum yield of $^1O_2$ production was observed for a bovine serum albumin (BSA) complex with [60]fullerene *tris*-malonic acid, the triplet lifetime of HSA-CF was significantly shortened, compared to the noncomplexed fullerene.[29]

On the basis of our previous studies, we wanted to evaluate the possibility of treating non-melanoma skin cancers using the [60]fullerene derivatives. Although our previous studies on pancreatic stellate cells using a water-soluble glycofullerene (*Sweet-*C_{60}) demonstrated that it was photoactive, no biophysical studies were performed and therefore its photochemistry remains unknown.[23] Here, the physicochemical properties of the neutral glycofullerene GF1 (a water-soluble analog of *Sweet-*C_{60}) and its peracetylated lipophilic analog MMS48 were compared with those of two cationic aminofullerenes— MomoaminoC_{60} and HexakisaminoC_{60} (Figure 1). The formation of singlet oxygen was confirmed by measuring its phosphorescence at 1270 nm in the presence and absence of albumin (BSA). Using EPR spin trapping and HPLC with electrochemical detection, we monitored cholesterol peroxidation and protein oxidation, which revealed that the synthesized fullerene nanomaterials were promising

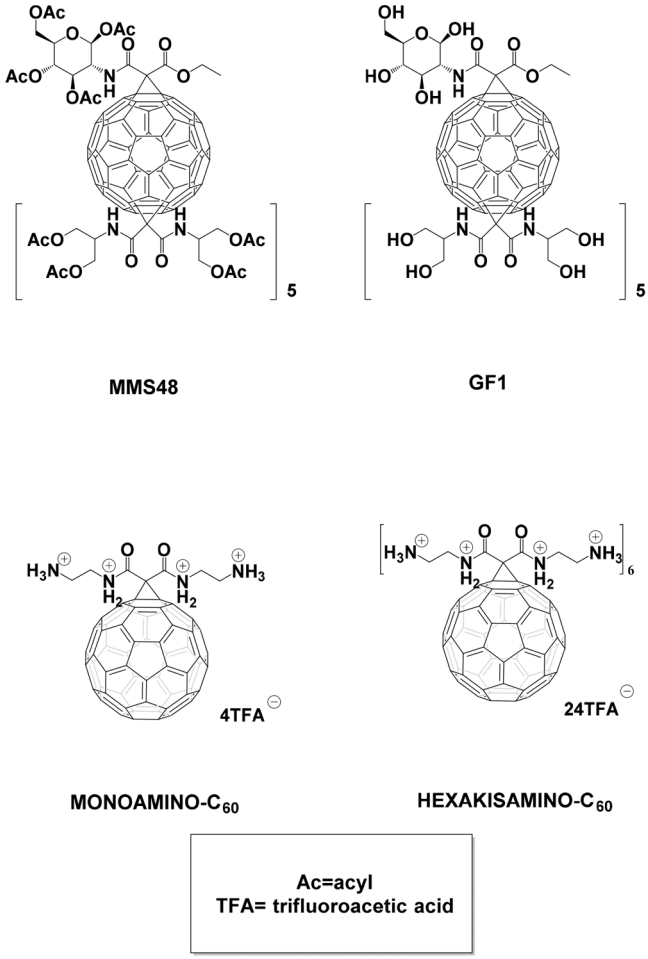

Figure 1. Chemical structures of the fullerenes GF1, MMS48, MONOAMINOC_{60}, and HEXAKISAMINOC_{60}.

photosensitizers that could be used in anticancer photodynamic therapy. Both singlet oxygen and oxygen radicals can cause oxidative damage to vital targets in cells by starting chain reactions of peroxidation in the cell membranes and disrupting the enzymatic or structural functions of proteins. Lipid and protein peroxides can also damage other important targets in cells.[30,31] The ability to cause photooxidized damage to cellular targets was confirmed using phototoxicity assays in a cellular model of squamous skin cancer.

EXPERIMENTAL SECTION

Materials. All of the compounds that were used were reagent grade or better and the solvents were used as-received, unless otherwise specified. The following reagents were used as-received: C_{60} (99.5%, SES RESEARCH, U.S.A.), 2-amino-1,3-propanediol (AK Scientific), DBU (1,8-diaza-bicyclo [5.4.0]undec-7-ene, Sigma-Aldrich), acetic anhydride (Acros Organics), malonic acid methyl ester (Acros Organics), CBr_4 (Sigma-Aldrich), EDCI hydrochloride [*N*-ethyl-*N*′-(3-(dimethylamino)propyl)carbodiimide hydrochloride, Acros Organics], *N*-hydroxysuccinimide (Sigma-Aldrich), potassium carbonate (Sigma-Aldrich), trifluoroacetic acid (Acros Organics), and trityl chloride (Acros Organics). All of the solvents that were used to prepare the fullerene nanomaterials were prepared according to the procedures in the literature by distilling them with calcium hydride and were used immediately. The nuclear magnetic resonance spectra were measured on a Bruker Avance III 500 MHz NMR Spectrometer with TMS as the internal standard. The MS spectra for the water-insoluble fullerenes were collected using an Autoflex II MALDI-TOF

https://dx.doi.org/10.1021/acsbiomaterials.0c00932
ACS Biomater. Sci. Eng. 2020, 6, 5930−5940

mass spectrometer, and for the water-soluble [60]fullerene derivatives, an MS electrospray ionization time-of-flight (ESI-microTOF) mass spectrometer was used; both instruments were from Bruker Daltonics Inc. (Fremont, CA, U.S.A.). The final dialysis purification of the water-soluble fullerene nanomaterials was performed on Pall Microsep centrifugal membranes with the molecular cutoffs at 1 and 3 kDa. The purity of all of the compounds was assessed using an Agilent1260, which was equipped with a DAAD detector at 260 nm and an RP-column: Eclipse plus C18 (3.5 μm); flow 0.5 mL/min. The Fourier transform infrared (FTIR) measurements were carried out using an Agilent Cary 640 FTIR spectrometer, which was equipped with a standard source and a DTGS Peltier-cooled detector. The aminofullerene powders were mixed with KBr and measured in the transmittance mode in the 400−4000 cm^{-1} range. The spectrum was recorded at 32 accumulations and a spectral resolution of 4 cm^{-1}. The obtained data were analyzed using the baseline, water and carbon dioxide corrections.

Synthesis of the [60]Fullerene Derivatives. The glycofullerenes MMS48 and GF1 were synthesized according to a previously described methodology.[24] The synthetic protocol for preparing the aminofullerenes (Monoamino-C_{60} and Hexakisamino-C_{60}) is depicted in Scheme S1 of the Supporting Information (SI), which presents the detailed NMR and mass spectrometry analyses, DLS, and zeta potential measurements (see SI).

N^1-Tritylethane-1,2-Diamine (1). Ethylenediamine (24.96 mmol; 1.5 g) was dissolved in 40 mL of dichloromethane, and then anhydrous potassium carbonate (24.96 mmol; 3.45 g) was added to the solution. Next, a trityl chloride solution (12.48 mmol 3.48 g) in DCM was added to the reaction mixture over 40 min and was stirred at room temperature for 3 days. After this time, the white solid was filtered off, and the obtained filtrate was extracted three times by adding 3 × 50 mL of deionized water. The organic phase was dried over magnesium sulfate and purified using column chromatography (DCM: MeOH, 10/1, *v*/*v*; R_f = 0.16). The final product was obtained as a white solid with a yield of 82% and mp as 93 °C.[32]

N^1,N^3-Bis(2-(tritylamino)ethyl)malonamide (2). Tritylethane-1,2-diamine (3.08 mmol; 0.93 g) was dissolved in 100 mL of methanol and then dimethyl malonate (1.5 mmol; 0.2 g) was added dropwise for 10 min. The obtained reaction mixture was refluxed for 3 h and then stirred at room temperature for 2 days to obtain a reddish solution of the desired malonate. After that time, the reaction mixture was evaporated, and the obtained brownish oil was dissolved in 50 mL methylene chloride and extracted three times with 50 mL of deionized water. The organic phase was evaporated, which produced the desired bismalonamide as a brown, oily product with a final yield of 69%, which was used for the further Bingel−Hirsch cyclopropanation reactions with no additional purifications (the high resolution mass spectrometry of malonate **2** is depicted in Figure S2 of the SI).

MonoaminoC_{60}. The fullerene C_{60} (0.5 mmol; 360 mg) was added to the freshly distilled toluene (450 mL), mixed for 5 min using a magnetic stirrer, which was followed by an additional suspension using an ultrasonic bath for 15 min (the temperature of the C_{60} solution did not exceed 50 °C). Then, a dichloromethane solution (10 mL) of bismalonamide **2** (0.5 mmol; 333.6 mg) and CBr_4 (1 mmol; 331.63 mg) was added to the solution of C_{60}, which was followed by the dropwise addition of a solution of DBU (0.625 mmol; 95.1 mg) in 5 mL of DCM; the reaction was allowed to stir for 2 h at room temperature. After that time, the fullerene monoadduct (**3**) was isolated using the two-step flash chromatography procedure. For this purpose, the reaction mixture was first purified on a precolumn using toluene as the mobile phase—the biggest fraction was from the unreacted fullerene. Then, the final product was eluted from the column using a mixture of CH_2Cl_2/MeOH 5:1 to 2:1. The brown filtrate was evaporated in vacuo to form a brown solid with a 28% yield and the structure of fullerene monoadduct (**3**), which was confirmed by NMR spectroscopy (see SI) as well as MALDI-TOF spectrometry (Figure S1). The final hydrolysis of trityl-protected fullerene monoadduct (**3**) was performed using a 20% dichloromethane solution of trifluoroacetic acid. Briefly, 200 mg of the fullerene monoadduct (**3**) was dissolved in a 20 mL mixture of DCM and 20% trifluoroacetic acid (1/1, *v*/*v*). The solution was stirred at room temperature for 7 days, during which the changes in the color of the aqueous layer from transparent to red-orange were observed. Next, 50 mL of water was added to the solution, and the phases were separated in a separatory funnel and the aqueous phase was collected and evaporated. The MonoaminoC_{60} was purified on centrifugal membranes using a 1 kDa filter membrane (Pall Corporation, U.S.A.), and the upper layer of the membrane was washed four times with 15 mL of distilled water. Then, the desired fullerene nanomaterial (**4**) was passed through syringe filters (0.2 μm) to sterilize it and to remove any larger agglomerates. The sample was then freeze-dried in a lyophilizer, which resulted in a reddish mesh powder that was stored at −20 °C. The desired MonoaminoC_{60} was characterized using NMR, infrared spectroscopy, and ESI−MS (see the SI).

HexakisaminoC_{60}. A fullerene monoadduct (**4**) (0.2 mmol; 278 mg) was dissolved in 10 mL of DCM and then 100 mL of toluene was added under intensive stirring at room temperature. In a separate 25 mL vial, 15 mL of a chloroform solution of malonate (**2**) (2 mmol; 1350 mg) and carbon tetrabromide (4 mmol; 1324 mg) was prepared. The contents of the vial were added to the solution of MonoaminoC_{60} for 5 min, after which, a 3 mL chloroform solution of DBU was prepared (362 mg; 2.4 mmol) to which 0.5 mL DBU solution was added every 60 min. Next, the reaction mixture was stirred at room temperature for 48 h, during which the color of the solution changed to orange. A [60]fullerene Hexakis adduct (**5**) was purified from the organic impurities using a flash column, first using methylene chloride and then eluting the final [60]fullerene derivative with an eluent that consisted of a mixture of DCM: MeOH (9:1, *v*/*v*) and then the final T_h symmetrical Hexakis adduct of [60]fullerene was concentrated on a rotary evaporator. The fullerene derivative (**5**) was characterized using NMR spectroscopy (See Supporting Information and Figure S1). In order to remove the trityl-protecting group from the fullerene nanomaterial (**5**), the compound was hydrolyzed using 20% trifluoroacetic acid. Briefly, a sample of the compound (**5**) was dissolved in a mixture of 10 mL DCM and 10 mL 20% TFA. The solution was stirred at room temperature for 7 days, during which the color of the aqueous layer changed from transparent to orange. Next, 25 mL of water was added to the fullerene solution, extracted and then the aqueous phase was collected and evaporated. The HexakisaminoC$_{60}$ was purified on centrifugal membranes using a 1 kDa filter membrane (Pall Corporation, U.S.A.), the top layer of the membrane was washed four times with 15 mL of distilled water and passed through syringe filters (0.2 μm) to sterilize it and to remove any larger agglomerates. The [60]fullerene nanomaterial was then frozen at −20 °C and freeze-dried, which resulted in a red powder that was then stored in a laboratory freezer at −20 °C. The HexakisaminoC$_{60}$ was characterized using NMR and infrared spectroscopy and was confirmed using ESI−MS.

Singlet Oxygen Phosphorescence and EPR Spin Trapping. The near-infrared luminescence (1270 nm) was measured perpendicular to the excitation beam in the photon-counting mode using a thermoelectric-cooled NIR PMT module (H10330−45; Hamamatsu, Japan), which was equipped with a 1100 nm cutoff filter and an additional dichroic narrow-band NBP filter, selectable from the spectral range of 1150−1355 nm (NDC Infrared Engineering Ltd., Essex, U.K.). The data were collected using a computer-mounted PCI-board multichannel scaler (NanoHarp 250; PicoQuant GmbH, Berlin, Germany). Data analysis, including the first-order luminescence decay, which was fitted using the Levenberg−Marquardt algorithm, was performed using custom-written software. The acquisition time for obtaining the singlet oxygen phosphorescence signals was 20 s. The EPR measurements were performed using a Bruker EMX-AA EPR spectrometer (Bruker BioSpin, Rheinstetten, Germany). The EPR samples were run using a microwave power of 10.6 mW, a modulation amplitude of 0.05 mT, center field 339.0 mT, scan width 8 mT, and scan time 21 s.

The phosphate-buffered (pD 7.4, 10 mmol) D_2O solutions of the fullerene nanomaterials and TMPyP were excited in a 1 cm-optical path quartz fluorescence cuvette (QA-1000; Hellma, Mullheim, Germany) using the monochromatic light pulses that were generated

https://dx.doi.org/10.1021/acsbiomaterials.0c00932
ACS Biomater. Sci. Eng. 2020, 6, 5930−5940

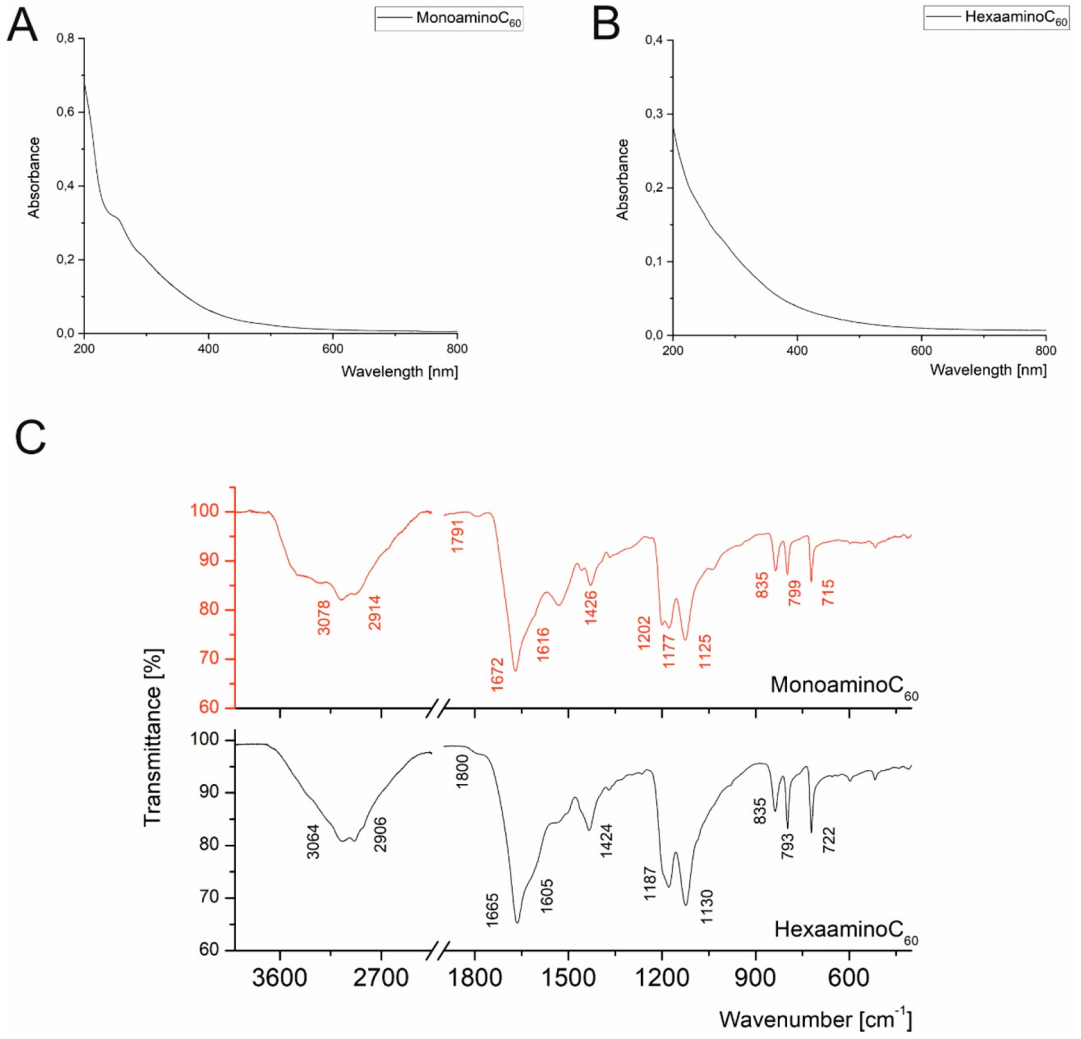

Figure 2. UV−vis and IR spectra of water-soluble [60]fullerenes MonoaminoC$_{60}$ and HexakisaminoC$_{60}$.

by an integrated nanosecond DSS Nd/YAG laser system, which was equipped with a narrow bandwidth optical parametric oscillator (NT242−1k-SH/SFG; Ekspla, Vilnius, Lithuania). The laser system delivered pulses at a 1-kHz repetition rate and had a pulse energy up to several hundred microjoules in the visible region and up to several tens of microjoules in the UVA−UVB region. The [60]fullerene photosensitizers were photoexcited using a 429 nm wavelength. The absorbance of the samples was set to 0.27 in that wavelength. In order to adjust the photoexcitation energy in the experiments, a laser beam was attenuated with three pieces of wire mesh (light transmission 40% each). The quantum yield of singlet oxygen formation was obtained using 5,10,15,20-tetrakis(1-methyl-4-pyridinio) porphyrin) *tetra*(*p*-toluenesulfonate) (TMPyP) as the reference compound (φ = 0.75).[33] For detection of radicals photogenerated by the studied [60]fullerens, EPR-spin trapping was employed, using DMPO as the spin trap at a concentration of 100 mM. Samples containing 0.1 mg/mL of appropriate fullerene nanomaterials in 80% DMSO were irradiated in EPR quartz flat cells in the resonant cavity with 402−508 nm (24 mW/cm^2) light, which was derived from a 300 W high-pressure compact arc xenon lamp (Cermax, PE300CE13FM/Module300W; PerkinElmer Optoelectronics, GmbH, Wiesbaden, Germany). To control spectral irradiance, the system was equipped with a water filter, heat reflecting hot mirror, cutoff filter that blocked light below 390 nm and a blue additive dichroic filter 505FD64−25 (Andover Corporation, Salem, NH, U.S.A.).

Photobleaching of HexakisaminoC$_{60}$. Stability of HexakisaminoC$_{60}$ was checked in PBS solution. Concentration was set to 0.05 mg/mL and absorbance spectra was recorded. The sample was irradiated with blue light from the same source and the same power flux as used for cell phototoxicity (445 nm, 20 mW/cm^2). Absorbance was measured in 5 min intervals to check if any changes occurred.

HPLC Monitored Cholesterol and Liposomes Peroxidation. The HPLC analysis and electrochemical detection on a mercury drop was employed for cholesterol hydroperoxides detection. This method enables identification and quantification of cholesterol hydroperoxides of different origin, thus allowing us to determine the major mechanisms of lipids oxidation.[34] 7$\alpha\beta$-OOH cholesterol hydroperoxides form as a result of cholesterol reaction with oxidizing radicals, while 5α-OOH and 6$\alpha\beta$-OOH hydroperoxides are generated *via* the reaction with singlet oxygen. In brief, multilayered liposomes were prepared from a mixture of DMPC/cholesterol in 3:1 molar ratio. Liposomes were enriched with [60]fullerenes in PBS solution during the creation from dry lipid layers, with one exception—fullerene nanomaterial MMS48 was added to chloroform solution of lipids, as it is totally water-insoluble, due to the presence of acetyl protecting groups. Liposomes were light-treated with 10 mW/cm^2 of blue light (445 nm), then lipids were extracted using modified Folch procedure, dried under nitrogen stream and frozen in −20 °C. For HPLC analysis the samples were dissolved in isopropanol and separated on RP-C$_{18}$ column. The mobile phase consisted of 72% methanol, 11% acetonitrile, 9% ultrapure H_2O (containing 1 mM of $NaClO_4$), and 8% of isopropanol. To determine retention times for cholesterol hydroperoxides (7α-OOH and 5α-OOH) analytical standards were used.

https://dx.doi.org/10.1021/acsbiomaterials.0c00932
ACS Biomater. Sci. Eng. 2020, 6, 5930−5940

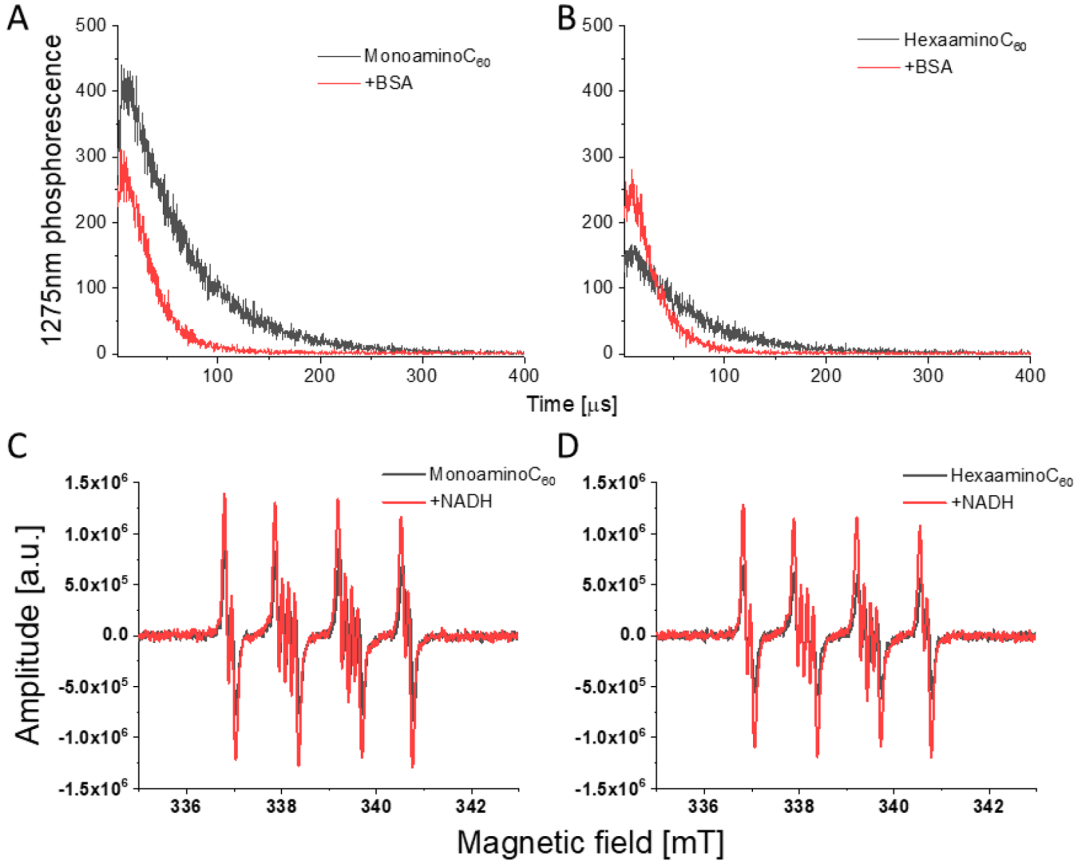

Figure 3. Singlet oxygen luminescence signals (A and B) after 429 nm laser pulse excitation observed in D_2O solutions of MonoaminoC$_{60}$ and HexakisaminoC$_{60}$ in absence (black lines) or with an addition of 35 μM of BSA (red line). DMPO spin trapping of respective C$_{60}$ in 80% of DMSO (C and D) without (black trace) or with addition of NADH (red trace).

Bovine Serum Albumin Oxidation Using CBA Test. Coumarin boronic acid (CBA) reacts with protein hydroperoxides forming fluorescent product 7-hydroxycoumarin (COH). This reaction can be used for quantification of protein oxidation.[35] Stock solution (2.5 mM) of bovine serum albumin (LabEmpire) was prepared in PBS directly before experiment and diluted to final concentration of 100 μM. HexakisaminoC$_{60}$ was added to samples to achieve desire concentrations of 50, 10, and 5 μg/mL. Protein hydroperoxide scavenger ebselen in concentration of 100 μM was added to one of the control samples.[36] Samples were placed in a 96-well plate (black, with bottom transparent) and irradiated with 20 mW/cm^2 blue light (blue COB led light, 445 nm) for 20 min. Just after irradiation 200 U of catalase was added for 5 min to all the samples to remove any hydrogen peroxide. CBA (final concentration 0.4 mM) in 10 times diluted PBS was added. Formation of fluorescent COH was monitored in 10 min intervals for 5 h using 360 (±15 nm) as excitation and 465 (±20 nm) as emission wavelength.

MTT Photocytotoxicity. Human squamous carcinoma A431 was obtained from the American Type Culture Collection (ATCC). The A431 cells were plated in 24-well plates at density of 35 000/well. Twenty-four hours after plating, the cells were incubated with high-glucose DMEM that contained HexakisaminoC$_{60}$ at different concentrations. Feeding was repeated two more times, at 24 h intervals. The day after the final feeding the cells were washed twice with PBS that contained calcium and magnesium ions, then irradiated for 15 min using a blue led light (440 nm) at a fluence rate of 20 mW/cm^2. Dark control cells were kept in the same conditions except for light exposure. After irradiation, the cells were provided by DMEM with 10% FBS. The cytotoxic effect of the photodynamic treatment was quantified 24 h after irradiation, using an MTT assay for the mitochondrial redox function. The MTT solution in DMEM with 10% FBS was added to the treated and control culture wells (final concentration of 0.5 mg/mL). After incubation for 30 min at 37 °C, the culture medium was removed, and the remaining blue precipitate was solubilized in DMSO, followed by reading the absorbance at 560 nm in a plate reader (GENios Plus, Tecan Austria GmbH). The results are reported as the percentage of the paired untreated controls. The experiments were repeated a minimum of three times.

Cellular PI Staining after PDT. To estimate the apoptotic effect of light induced HexakisaminoC$_{60}$, A431 cells were stained using fluorescent dye propidium iodide (PI) 24 h after irradiation, as described in a previously described protocol.[37] In brief, propidium iodide (final concentration 100 μM) was added to the control and treated cells, and fluorescence images (510−560 nm excitation/580 nm emission) were taken to detect PI-positive nuclei. Then, Triton X-100 was added (final concentration 0.1%), and fluorescence images were captured to quantify the total cell number in each field. The number of viable cells and the total number of cells per field were quantified using the ImageJ software with the Huang method[38] for cell finding using a custom-written script by Dr. Łukasz Bujnowicz (Jagiellonian University, Poland).

RESULTS AND DISCUSSION

Chemistry. *Synthesis and Physicochemical Properties of Aminofullerenes MonoaminoC$_{60}$ and HexakisaminoC$_{60}$.* On the basis of previously reported literature findings describing the use of fullerene nanomaterials in photodynamic therapy, we aimed to synthesize water-soluble [60]fullerene photosensitizers possessing multiamino groups, which are easily assessable utilizing a trityl function protection/deprotection approach. The fullerene scaffold has great potential to be chemically modified, enhancing its water-solubility, therefore

https://dx.doi.org/10.1021/acsbiomaterials.0c00932
ACS Biomater. Sci. Eng. 2020, 6, 5930−5940

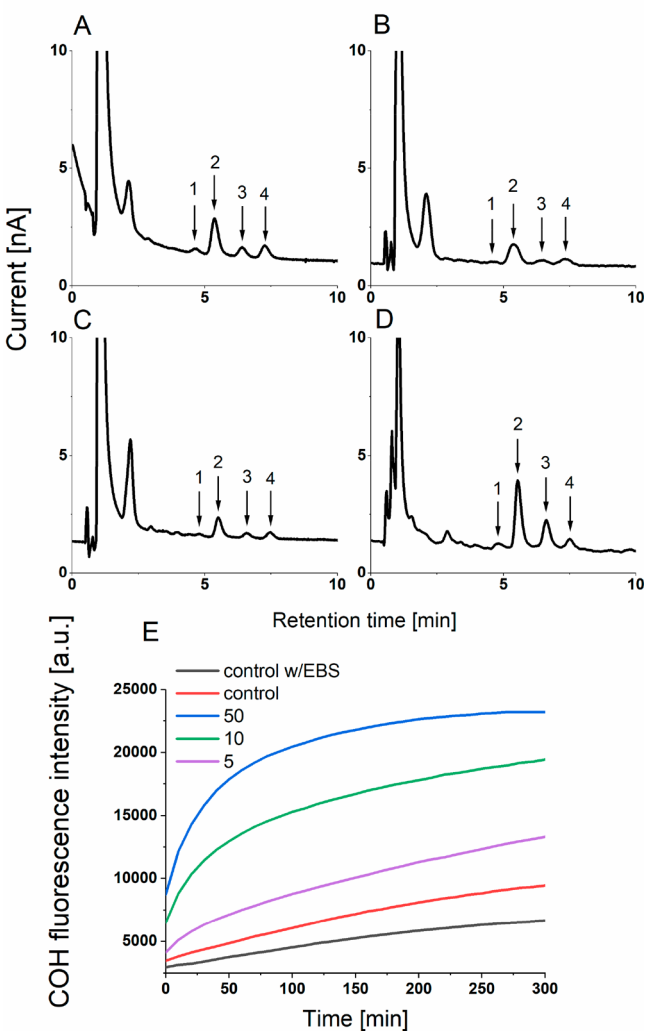

Figure 4. HPLC chromatograms of DMPC/cholesterol liposomes with four [60]fullerene derivatives (A, HexakisaminoC$_{60}$; B, MonoaminoC$_{60}$; C, GF1; D, MMS48). The arrows indicate the cholesterol hydroperoxides with their characteristic retention times (1, 4.7 min—7$\alpha\beta$-OOH; 2, 5.5 min—5α-OOH; and 3 and 4, 6.6 and 7.5 min—6$\alpha\beta$-OOH), respectively. Panel E shows the formation of the protein hydroperoxides that were determined using COH.

the Bingel−Hirsh approach gives a possibility to modify its structure with specially designed malonates, thanks to the ability to control the cyclopropanation reaction and obtaining selected regioisomers, especially [60]fullerene monoadducts and Hexakisadducts with T_h symmetry. This phenomenon was especially important for our biophysical comparative studies, because less substituted fullerenes seem to be more effective photosensitizers based on the studies performed by Hamblin et al.[17,39] However, tailored designed [60]fullerene derivatives might be hard to accomplish, due to variations of the degree of malonate additions and complex addition patterns. To address these problems, we propose the use of malonamide (**2**) in the double Bingel-Hirsh protocol.[23] The molecular ion peak of compound (**2**) was observed in the high resolution ESI mass spectrum at 673.3536 Da (calculated for $C_{45}H_{45}N_4O_2$, 673.35425 Da, Figure S3). The time-controlled reaction is stopped after 2 h to prevent formation on bisadduct regioisomers or used further for creation of highly symmetrical Hexakisadducts from more reactive monoadducts. An overview of whole synthetic strategy is depicted in Scheme S1 (see SI), starting with ethylenediamine core, we aimed to obtain trityl based symmetrical malonamide (**2**), but without using additional coupling agents, only by a gentle refluxing with dimethyl malonate. For all water-soluble fullerene nanomaterials ESI-spectrometry was used for detection of molecular peaks, but trityl-protected [60]fullerenes were measured by MALDI-TOF technique using DCTB matrix. The formation of [60]fullerene monoadduct (**3**) was confirmed by ^{13}C NMR spectroscopy based on its molecular symmetry (Figure S1, characteristic C_{60} signals from 2 × 15 sp^2 carbon atoms between 145 and 139 ppm and one sp^3 carbon at 70.4 ppm) and MALDI-TOF mass spectrometry with a molecular ion peak at 1436.309 Da (M−H+2Na, Figure S4, M−H+2Na). The desired MonoaminoC$_{60}$ was obtained by deprotection of trityl groups in 20% TFA, followed by membrane dialysis with 1 kDa cutoff. It was further characterized by NMR spectroscopy and positively ionization ESI−MS with observed molecular ion peak 478.86 Da [M + H]$^{2+}$ (Figure S5). Next, a highly symmetrical [60]fullerene Hexakisadduct (**5**) was created using fullerene monoadduct (**3**) as a starting material, in a second Bingel−Hirsh reaction with an 10-fold excess of malonate (**2**) and CBr_4 and controlled addition of DBU during 6 h. This double Bingel−Hirsh synthetic approach to [60]fullerene Hexakisadducts was described by our group earlier and generates increased yields of final products as well as reduced presence of different regioisomers in the reaction mixture (mainly tris- and tetrakisadducts as byproducts). The T_h symmetry of [60]fullerene Hexakisadduct (**5**) was confirmed by ^{13}C NMR spectroscopy, which is expressed by a reduction of fullerene sp^2 signals in the carbon spectrum. Only two signals (143.97 and 142.62 ppm) of fullerene sp^2 carbons and one sp^3 carbon of cyclopropane ring (70.4 ppm) could be observed in the carbon spectrum of Hexakisadduct (**5**) (Figure S2). The aforementioned hydrolysis protocol was carried out to obtain HexakisaminoC$_{60}$ from a corresponding trityl protected fullerene derivative (**5**) and the desired water-soluble [60]fullerene (**6**) was characterized by NMR spectroscopy and ESI mass spectrometry with detected molecular ion peak at 1839.3 Da (positive mode, 50 mV, [M+2H]$^+$, Figure S6A). The change of experimental setup during electrospray spectrometry measurements (to 300 mV voltage), resulted in a rapid fragmentation of HexakisaminoC$_{60}$, with observed molecular ion peak of a parent MonoaminoC$_{60}$ disodium fragment [M+2Na+H_2O]$^+$.

The UV−vis spectra of two water-soluble aminofullerenes are presented in the Figure 2A,B. This experimental observation could be also partially explained by higher water solubility of HexakisaminoC$_{60}$ (above 250 mg/mL) in comparison to MonoaminoC$_{60}$ (around 30 mg/mL).

In the case of MonoaminoC$_{60}$, one characteristic absorption peak could be observed at 270 nm. This local maximum is similar to the UV absorption spectra of pristine C_{60} fullerene in a toluene solution (maxima observed at 269 nm), with only minimal absorption below 550 nm and negligible fluorescence. In electron spectrum of Hexakisadduct (**6**) no clear maxima was observed, which was also described for water-soluble glycofullerenes and other aminofullerenes.[23,40] Additionally, for the same concentrations of aminofullerenes, the HexakisaminoC$_{60}$ spectrum was hypochromized for a given absorbance on the order of 45%, which may be explained by formation of [60]fullerene aggregates. The DLS measurements performed on a Malvern Zetasizer illustrate that both aminofullerenes

https://dx.doi.org/10.1021/acsbiomaterials.0c00932
ACS Biomater. Sci. Eng. 2020, 6, 5930−5940

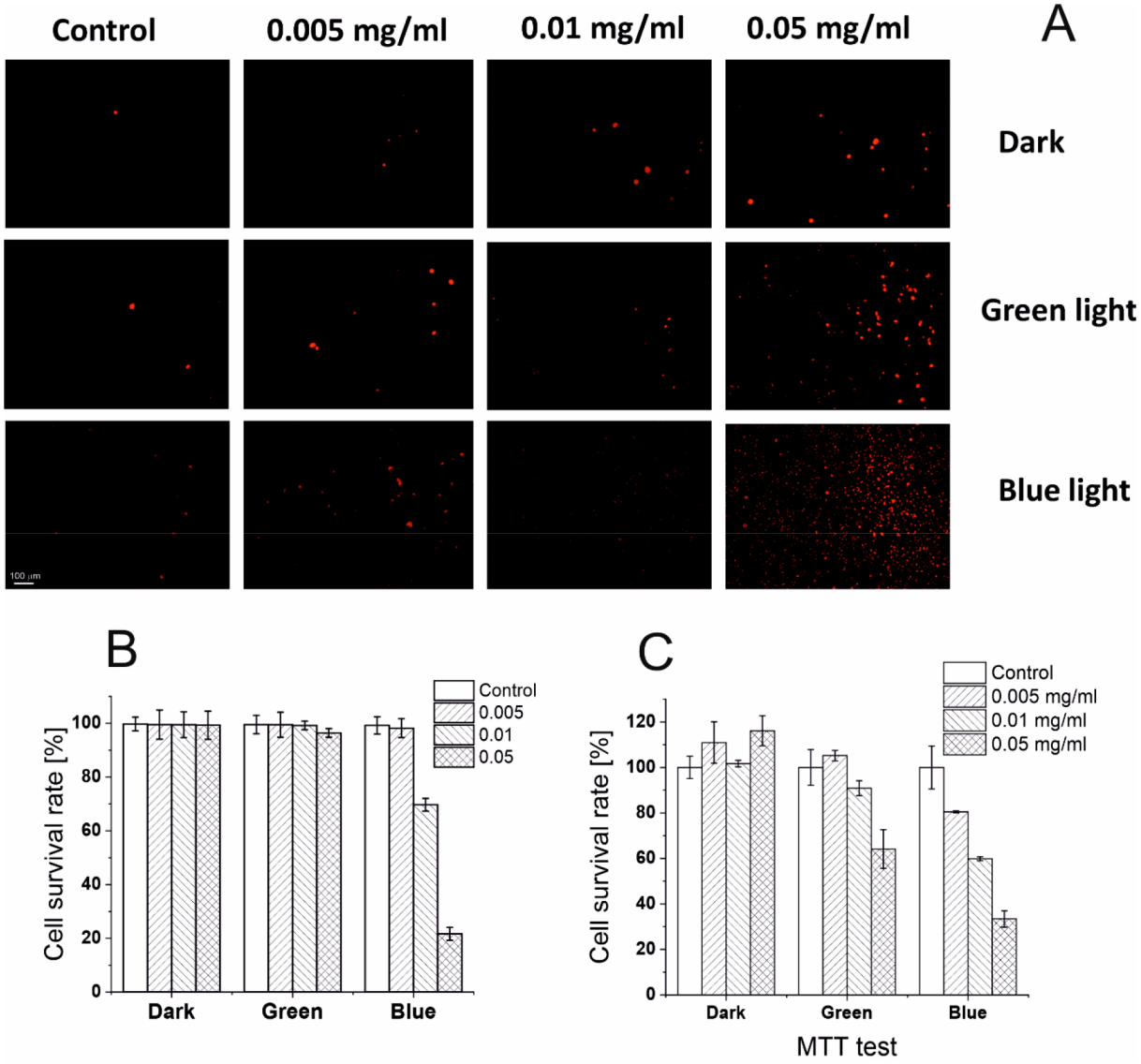

Figure 5. Microscopic images of the phototreated A431 cells that had been stained with propidium iodide (A); the results that were obtained after a mathematic picture analysis (B) of the same experiment, which was recalculated for cell survivability. The result of the MTT assay of the A431 cells after irradiation (C); and different bars show the different HexakisaminoC_{60} concentrations.

form aggregates, which are in a dynamic equilibrium as described previously for fullerene Hexakisadduct C_{60} ser.[41] The MonoaminoC_{60} forms larger aggregates around 354 nm with observed zeta potential at +31 mV; in contrast HexakisaminoC_{60} seems to predominantly aggregate around 99 nm, indicating a surface of charge of +29 mV. Both aminofullerenes present a relatively good degree of stability, and the smaller aggregates and possibly a different morphology of Hexakisadduct aggregates may be partially explained by a different critical packing parameter *p*.[42]

The infrared spectra of engineered water-soluble fullerenes (MonoaminoC_{60} and HexakisaminoC_{60}) have been analyzed considering two spectral regions: (1) 2250−3800 cm^{-1} and (2) 400−1900 cm^{-1} (Figure 2C). The bands arrangement found in relation to the HexakisaminoC_{60} and MonoaminoC_{60} are quite similar, wherein small differences as for the number of bands, their intensity, or positions result from the number of functional groups anchored to the fullerene scaffold. Looking more precisely on the spectrum of Hexakisamino derivative of C_{60}, region 1 is linked mainly to the overlapping signals originating from the symmetric and asymmetric stretching modes of $\nu(CH_2)$ and $\nu(NH_x)$ (x = 2,3). The band positions of amine groups (3064 and 2906 cm^{-1}) relating to the band position of the typical amine result probably from the presence of inter- or intramolecular interactions.[43] Similarly affected seems to be the position of the methylene bands which may be shifted toward higher wavenumbers due to the presence of positive charge located on the amine groups, in relation to a typical position of the methylene group within the alkene chain.[44,45]

An interesting phenomenon is also observed for the whole band arrangement of region 1, where bands are characterized by the high full width at half-maximum and high intensity, indicating a huge distribution and high number of H-bonds with different donor−acceptor bonds lengths. According to this assumption, weak, medium, and strong hydrogen bonds are present, probably due to the high dynamicity of the system as well as the presence of TFA counterion, enforcing formation of the highly dynamic systems maintained by the H-bonding system. A slightly different situation appeared in the case of

https://dx.doi.org/10.1021/acsbiomaterials.0c00932
ACS Biomater. Sci. Eng. 2020, 6, 5930−5940

aminofullerene monoadduct. Here, the position of two additional bands found at higher wavenumbers is closely related to the symmetric and asymmetric stretching modes of amine groups, typically reported in the literature for free or weakly involved in the hydrogen bonding scheme, NH_2 groups. The other two bands observed in this region are slightly shifted toward higher wavenumbers in relation to the Hexakis aminofullerene, wherein its interpretation is similar like previously. As a result of such observations, the band arrangement of monoamino C_{60} may result from a much smaller number of functional units anchored to the fullerene core and their weaker influence in formation of the H-bonding.

The fingerprint (1) region of HexakisaminoC$_{60}$ fullerene, especially at high wavenumbers is characterized by one maximum, strong in the intensity centered at 1665 cm^{-1}, as well as a shoulder at 1605 cm^{-1} and one band low in the intensity located at 1800 cm^{-1}. All of those bands are linked to the stretching vibration of carbonyl moieties, whereby their positions are indicated on the primary amides located within the organic chain (Figure 2).[46] The position of low lying carbonyl bands may be explained two ways, as a result of the presence of hydrogen bonds or due to the occurrence of the β-diketone structure.[47,48]

In turn, the low intensity band centered at 1800 cm^{-1} might explain taking into account counterion in which the halogen atoms are directly bonded to a carbonyl group that according to the theory absorb strongly at the presence of fluorine. Other bands with the maxima at 1424, 1187, and 1130 cm^{-1} may respectively be linked to the symmetric deformational modes of ethylenediamine groups, as well as skeletal vibration of alkane chain and deformational modes of methylene groups. In turn, the group of bands centered at 835, 793, 722 cm^{-1} are difficult in the interpretation, because of the overlapping character of various modes which may be activated at those wavenumbers. However, those bands may try to interpret as the asymmetric deformation modes of tertiary amides at 835 cm^{-1}, the deformational mode within straight-chain alkanes at 793 cm^{-1} and CF at 726 cm^{-1}. A lower number of functional units anchored to the fullerene core, resulted in some shift of bands toward lower or higher wavenumbers, i.e., a shift of carbonyl moieties, strongly involved in the formation of the H-bonding scheme is correlated with the weakening of mutual interaction between donor−acceptor units. One can conclude that the smaller number of functional units anchored to the fullerene core, the weaker interaction between them could be observed. In addition, the position of bands linked to the modes corresponding to the ethylenediamine or the alkane chain is only slightly changed relating to the HexakisaminoC$_{60}$ but reveal the spatial rearrangement of this kind of functional groups.

Biophysics. The ability to cause photoinduced damage is a primary function of traditional as well as nanomaterial-based photosensitizers. In this study, we have shown that all four [60]fullerenes are able to produce reactive oxygen species (ROS). As depicted in Figure 3CD, the EPR spectra of spin adducts characteristic to spin trapping of superoxide anion by DMPO are being presented[49] (for a simulated spectrum of DMPO−OOH adduct see SI Figure S21). Efficiency of that process was markedly increased by the presence of an external electron donor like NADH (Figures 3CD, red traces). Although superoxide anion is not a very reactive compound, it can travel long distances inside cells and secondary reactions may oxidize targets far from its generation site. Singlet oxygen O_2 ($^1\Delta_g$), however, is much more reactive and in cellular environment could react in close vicinity to its point of formation. Singlet oxygen formation was detected by a direct observation of a characteristic phosphorescence of $O_2(^1\Delta_g)$ at 1275 nm in photon-counting mode (Figure 3AB). Experiments were conducted in phosphate D_2O buffer to increase the lifetime of the generated singlet oxygen and to enhance the detection sensitivity.[50] The quantum yield of singlet oxygen photogeneration for both aminofullerenes was obtained using TMAP as a standard and it was determined to be around 0.1 and 0.062 (HexakisaminoC$_{60}$ *vs* MonoaminoC$_{60}$, Figures S12 and S18); in the case of MMS48, the tetraphenylporphirine (TPP) was used as a standard, in a chloroform solution (Figure S20). Although it is not a high yield for HexakisaminoC$_{60}$, in the presence of serum albumin the formation of singlet oxygen was markedly increased (Figure 3B), what was also measured quantitively (Figure S22). As expected, lifetime of singlet oxygen decreased in the presence of albumin, due to reaction with the protein (the corresponding rate constant being around 7×10^8).[51] The elevated efficiency of singlet oxygen photogeneration observed for HexakisaminoC$_{60}$−BSA complex, compared to HexakisaminoC$_{60}$ alone is noteworthy. Typically, complexation of a photosensitizer molecule by albumin is accompanied by substantial reduction in the photosensitizer efficiency to photogenerate singlet oxygen. Such a phenomenon has been observed for WST-11 and WST-19 photosensitizers.[52,53] The increased efficiency of photogeneration of singlet oxygen by HexakiskisaminoC$_{60}$−BSA, compared to MonaminoC$_{60}$−BSA remains rather puzzling, suggesting different mechanism of BSA binding. This may be caused by a different mode of binding affinities of synthesized aminofullerenes to IIA and IIIA subdomains of BSA. The larger and more substituted and T_h symmetrical HexakisaminoC$_{60}$ could be easier to bind to hydrophobic pockets of BSA. Moreover, the computational studies performed by the group of Papadopoulos indicated that positively charged aminofullerens and fullerene carboxylic acids that negatively charged groups attached to the fullerene core may be necessary to enhance ligand−HAS interactions.[54] Only a limited number of cationic compounds have been reported to exempt this rule—this observation may be true for fullerene nanomaterial HexakisaminoC$_{60}$, but further computational studies should be performed. Moreover, a recent studies by Di Giosia *et al.* have also reported the shielding effects of proteins in the case of C$_{60}$@lysozyme hybrid, which was visualized by the increase in singlet oxygen generation and reduction of quenching by water molecules.[55,56] In our case, HexakisaminoC$_{60}$ is forming smaller aggregates than MonoaminoC$_{60}$ (99 nm *vs* 354 nm), which may also favor its better ability to produce $^1O_2$ after binding with BSA.

The analysis of cholesterol peroxidation products induced by the studied [60]fullerenes reveal that at least in liposomes, the main oxidizing species is singlet oxygen (Figure 4ABCD). The peak from 7ab-OOH (depicted in Figure 4 as **1**, with a retention time of 4.7 min) is barely visible and could come from internal rearrangements of singlet oxygen-related hydroperoxides.[34] It would suggest that in a lipid microenvironment, the excited triplet states of fullerene nanomaterials are much more prone to energy transfer, resulting in singlet oxygen production. This effect is especially pronounced for the water insoluble form—MMS48 (Figure 4D). From three tested water-soluble fullerene derivatives, HexakisaminoC$_{60}$ was found to be most effective in the photooxidation of cholesterol

https://dx.doi.org/10.1021/acsbiomaterials.0c00932
ACS Biomater. Sci. Eng. 2020, 6, 5930−5940

(Figure 4A). Additionally, HexakisaminoC_{60} nanomaterial, as well as other tested fullerene nanomaterials were found to be quite resistant to photobleaching in conditions used for photodynamic treatment (Figures S14−S17). As for cellular and tissue applications, the presence of serum albumin is inevitable, we have chosen HexakisaminoC_{60} derivative for further studies in cell phototoxicity experiments using squamous skin carcinoma model. The ability to photooxidize proteins by Hexakis derivative of C_{60} was further investigated using coumarin boronic acid assay (Figure 4E). The obtained results clearly show a dose-dependent increase in the amount of fluorescent COH, which is a product of reaction of nonfluorescent CBA and bovine serum albumin hydroperoxides. This observation confirms that during blue LED light irradiation, HexakisaminoC_{60} is able to also oxidize proteins.

Photodynamic Therapy. To determine cell phototoxicity, the A431 cell line of a non-melanoma skin cancer was used. The cells were fed with HexakisaminoC_{60} fullerene for three consecutive days. During that time, no dark toxicity in the range of the concentrations that were used in the experiment was observed (Figure 5). Phototoxicity was pronounced for the cells that were irradiated with blue light (445 nm), while a significantly weaker effect was observed when the cells were irradiated with green light (500−580 nm). This observation is consistent with the relative absorbance of the C_{60} derivatives. Two methods were used to detect phototoxicity—determining the mitochondrial activity (MTT assay, Figure 5C) and cell membrane permeability (propidium iodide test, Figure 5AB). Although the observed effects for both tests were photosensitizer-dose dependent, the MTT test produced more pronounced results that showed photodynamic damage, which may suggest that the photoinduced damage primarily occurs in the cell mitochondria and cytosol. This observation is in agreement with previous studies on glycofullerenes as well as with the fluorescently labeled fullerene derivative C_{60} serPF, which have demonstrated that water-soluble [60]fullerene derivatives tend to accumulate mainly in the nuclear envelope and cytosol of cancer cells.[23,57] The green light exposure caused negligible effects in the membrane permeability assay even at the highest concentration of the nanophotosensitizer that was used, while for the same conditions, the cell viability that was measured by the MTT test was reduced to 60% (Figure 5). In both of those experiments, the blue LED light irradiation resulted in a substantial increase in cell death with a 0.05 mg/mL concentration of HexakisaminoC_{60} reducing the cell survival rate to around 20%. It was expected that there would be a lower efficiency under green light irradiation compared to the effective absorbance of HexakisaminoC_{60} in the corresponding regions of the absorbance spectrum. Although blue light has a low tissue penetration, in potential *in vivo* application, it can enable very precise targeting, which would reduce the damage to non-malignant tissues.[58] The results that were obtained using blue light irradiation clearly showed that this compound has the properties of a promising photosensitizer that could be used in topical applications.

CONCLUSIONS

We synthesized two novel aminofullerenes—MonoaminoC_{60} and HexakisaminoC_{60} and compared their biophysical properties based on studies of ROS formation, and lipid and protein peroxidation. On the basis of the observation that BSA−HexakisaminoC_{60} complex increased the formation of singlet oxygen, we selected HexakisaminoC_{60} for further cellular studies, which confirmed its high phototoxicity, which had negligible effects without LED irradiation. Additionally, we do believe that further molecular docking studies should also be performed to visualize differences of BSA binding to a different [60]fullerene derivatives. The future 3D-spheroid or *in ovo* experiments should be performed to evaluate it as a photosensitizer in the photodynamic therapy of skin cancer, especially using a higher concentration of the [60]fullerene derivative and green LED irradiation due to its higher tissue penetration properties.

ASSOCIATED CONTENT

Supporting Information

The Supporting Information is available free of charge at https://pubs.acs.org/doi/10.1021/acsbiomaterials.0c00932.

Chemistry: Synthetic protocol for obtaining monoaminoC_{60} and hexakisaminoC_{60}; NMR of substrates and fullerene derivatives; high resolution ESI mass spectrometry of malonate (2); MALDI-TOF mass spectrometry of water insoluble fullerene (3); ESI mass spectrometry of water-soluble aminofullerenes (4) and (6); DLS studies of water-soluble aminofullerenes (4) and (6); Zeta potential measurements of water-soluble aminofullerenes (4) and (6); HPLC chromatogram of peroxides standards used for lipid peroxidation studies; Biophysics: quantum yield of singlet oxygen formation of hexakisaminoC_{60} (6); EPR spin trapping and singlet oxygen phosphorescence measurements for GF1; and photobleaching of HexakisaminoC_{60} (PDF)

AUTHOR INFORMATION

Corresponding Author

Maciej Serda − *Institute of Chemistry, University of Silesia in Katowice, Katowice 40-007, Poland;* orcid.org/0000-0003-4926-5782; Email: maciej.serda@us.edu.pl

Authors

Grzegorz Szewczyk − *Faculty of Biochemistry, Biophysics, and Biotechnology, Jagiellonian University, Kraków 30-387, Poland*

Olga Krzysztyńska-Kuleta − *Faculty of Biochemistry, Biophysics, and Biotechnology, Jagiellonian University, Kraków 30-387, Poland*

Julia Korzuch − *Institute of Chemistry, University of Silesia in Katowice, Katowice 40-007, Poland*

Mateusz Dulski − *Institute of Materials Engineering and Silesian Center for Education and Interdisciplinary Research, University of Silesia in Katowice, Chorzów 41-500, Poland*

Robert Musioł − *Institute of Chemistry, University of Silesia in Katowice, Katowice 40-007, Poland*

Tadeusz Sarna − *Faculty of Biochemistry, Biophysics, and Biotechnology, Jagiellonian University, Kraków 30-387, Poland*

Complete contact information is available at: https://pubs.acs.org/10.1021/acsbiomaterials.0c00932

Author Contributions

Design, conceptualization, and methodology: M.S., G.S.; chemical synthesis and characterization: M.S., J.K., and M.D.; Biophysical measurements: G.S.; Cellular experiments: O.K.K.; Writing and editing: M.S., G.S., R.M., and T.S.

Notes

The authors declare no competing financial interest.

https://dx.doi.org/10.1021/acsbiomaterials.0c00932
ACS Biomater. Sci. Eng. 2020, 6, 5930−5940

■ ACKNOWLEDGMENTS

M.S. thanks the National Science Center (Poland) for its support (Grant SONATA UMO-2016/23/D/NZ7/00912). M.D. is thankful for financial support from the National Science Center that was based on decision 2017/26/D/ST8/01117. Additionally, the authors want to thank Dr. Bujnowcz for his custom-written script for cell image analysis and Institute of Applied Radiation Chemistry from Lodz University of Technology (Poland) for providing us CBA probe.

■ REFERENCES

(1) Apalla, Z.; Lallas, A.; Sotiriou, E.; Lazaridou, E.; Ioannides, D. Epidemiological trends in skin cancer. *Dermatology practical & conceptual* **2017**, *7* (2), 1.

(2) Didona, D.; Paolino, G.; Bottoni, U.; Cantisani, C. Non melanoma skin cancer pathogenesis overview. *Biomedicines* **2018**, *6* (1), 6.

(3) Ting, P. T.; Kasper, R.; Arlette, J. P. Metastatic basal cell carcinoma: report of two cases and literature review. *J. Cutaneous Med. Surg.* **2005**, *9* (1), 10−15.

(4) Toll, A.; Margalef, P.; Masferrer, E.; Ferrándiz-Pulido, C.; Gimeno, J.; Pujol, R. M.; Bigas, A.; Espinosa, L. Active nuclear IKK correlates with metastatic risk in cutaneous squamous cell carcinoma. *Arch. Dermatol. Res.* **2015**, *307* (8), 721−729.

(5) Bastian, B. C. The molecular pathology of melanoma: an integrated taxonomy of melanocytic neoplasia. *Annu. Rev. Pathol.: Mech. Dis.* **2014**, *9* (1), 239−271.

(6) Apalla, Z.; Nashan, D.; Weller, R. B.; Castellsague, X. Skin cancer: epidemiology, disease burden, pathophysiology, diagnosis, and therapeutic approaches. *Dermatology and therapy* **2017**, *7* (1), 5−19.

(7) Christensen, E.; Warloe, T.; Kroon, S.; Funk, J.; Helsing, P.; Soler, A.; Stang, H.; Vatne, Ø.; Mørk, C. Guidelines for practical use of MAL-PDT in non-melanoma skin cancer. *J. Eur. Acad. Dermatol. Venereol.* **2010**, *24* (5), 505−512.

(8) Jung, S. K.; Lee, K. W.; Byun, S.; Kang, N. J.; Lim, S. H.; Heo, Y.-S.; Bode, A. M.; Bowden, G. T.; Lee, H. J.; Dong, Z. Myricetin suppresses UVB-induced skin cancer by targeting Fyn. *Cancer Res.* **2008**, *68* (14), 6021−6029.

(9) Cranmer, L. D.; Engelhardt, C.; Morgan, S. S. Treatment of unresectable and metastatic cutaneous squamous cell carcinoma. *Oncologist* **2010**, *15* (12), 1320.

(10) Safwat, M. A.; Soliman, G. M.; Sayed, D.; Attia, M. A. Fluorouracil-loaded gold nanoparticles for the treatment of skin cancer: development, in vitro characterization, and in vivo evaluation in a mouse skin cancer xenograft model. *Mol. Pharmaceutics* **2018**, *15* (6), 2194−2205.

(11) Petrilli, R.; Eloy, J. O.; Saggioro, F. P.; Chesca, D. L.; de Souza, M. C.; Dias, M. V.S.; daSilva, L. L.P.; Lee, R. J.; Lopez, R. F.V. Skin cancer treatment effectiveness is improved by iontophoresis of EGFR-targeted liposomes containing 5-FU compared with subcutaneous injection. *J. Controlled Release* **2018**, *283*, 151−162.

(12) Shi, L.; Wang, X.; Tu, Q.; Wang, H.; Zhang, H.; Wang, P.; Zhang, L.; Huang, Z.; Wang, X.; Zhao, F.; Luan, H. Treating cutaneous squamous cell carcinoma using 5-aminolevulinic acid polylactic-co-glycolic acid nanoparticle-mediated photodynamic therapy in a mouse model. *Int. J. Nanomed.* **2015**, *10*, 347.

(13) Huang, P.; Xu, C.; Lin, J.; Wang, C.; Wang, X.; Zhang, C.; Zhou, X.; Guo, S.; Cui, D. Folic acid-conjugated graphene oxide loaded with photosensitizers for targeting photodynamic therapy. *Theranostics* **2011**, *1*, 240.

(14) Zhu, Z.; Tang, Z.; Phillips, J. A.; Yang, R.; Wang, H.; Tan, W. Regulation of singlet oxygen generation using single-walled carbon nanotubes. *J. Am. Chem. Soc.* **2008**, *130* (33), 10856−10857.

(15) Mroz, P.; Pawlak, A.; Satti, M.; Lee, H.; Wharton, T.; Gali, H.; Sarna, T.; Hamblin, M. R. Functionalized fullerenes mediate photodynamic killing of cancer cells: Type I versus Type II photochemical mechanism. *Free Radical Biol. Med.* **2007**, *43* (5), 711−719.

(16) Mroz, P.; Tegos, G. P.; Gali, H.; Wharton, T.; Sarna, T.; Hamblin, M. R. Photodynamic therapy with fullerenes. *Photochemical & Photobiological Sciences* **2007**, *6* (11), 1139−1149.

(17) Hamblin, M. R. Fullerenes as photosensitizers in photodynamic therapy: pros and cons. *Photochemical & Photobiological Sciences* **2018**, *17* (11), 1515−1533.

(18) Lee, J.; Mackeyev, Y.; Cho, M.; Li, D.; Kim, J.-H.; Wilson, L. J.; Alvarez, P. J. Photochemical and antimicrobial properties of novel C60 derivatives in aqueous systems. *Environ. Sci. Technol.* **2009**, *43* (17), 6604−6610.

(19) Cho, M.; Lee, J.; Mackeyev, Y.; Wilson, L. J.; Alvarez, P. J.; Hughes, J. B.; Kim, J.-H. Visible light sensitized inactivation of MS-2 bacteriophage by a cationic amine-functionalized C60 derivative. *Environ. Sci. Technol.* **2010**, *44* (17), 6685−6691.

(20) Liu, Y.; Jiao, F.; Qiu, Y.; Li, W.; Lao, F.; Zhou, G.; Sun, B.; Xing, G.; Dong, J.; Zhao, Y.; et al. The effect of Gd@ C82 (OH) 22 nanoparticles on the release of Th1/Th2 cytokines and induction of TNF-α mediated cellular immunity. *Biomaterials* **2009**, *30* (23−24), 3934−3945.

(21) Guan, M.; Zhou, Y.; Liu, S.; Chen, D.; Ge, J.; Deng, R.; Li, X.; Yu, T.; Xu, H.; Sun, D.; et al. Photo-triggered gadofullerene: enhanced cancer therapy by combining tumor vascular disruption and stimulation of anti-tumor immune responses. *Biomaterials* **2019**, *213*, 119218.

(22) Hamblin, M. R. Upconversion in photodynamic therapy: plumbing the depths. *Dalton Transactions* **2018**, *47* (26), 8571−8580.

(23) Serda, M.; Ware, M. J.; Newton, J. M.; Sachdeva, S.; Krzykawska-Serda, M.; Nguyen, L.; Law, J.; Anderson, A. O.; Curley, S. A.; Wilson, L. J.; Corr, S. J. Development of photoactive Sweet-C60 for pancreatic cancer stellate cell therapy. *Nanomedicine (London, U. K.)* **2018**, *13* (23), 2981−2993.

(24) Serda, M.; Malarz, K.; Mrozek-Wilczkiewicz, A.; Wojtyniak, M.; Musioł, R.; Curley, S. A. Glycofullerenes as non-receptor tyrosine kinase inhibitors-towards better nanotherapeutics for pancreatic cancer treatment. *Sci. Rep.* **2020**, *10* (1), 1−11.

(25) Simões, M. F.; Sousa, J. S.; Pais, A. C. Skin cancer and new treatment perspectives: A review. *Cancer Lett.* **2015**, *357* (1), 8−42.

(26) Chen, Y.; Miclea, R.; Srikrishnan, T.; Balasubramanian, S.; Dougherty, T. J.; Pandey, R. K. Investigation of human serum albumin (HSA) binding specificity of certain photosensitizers related to pyropheophorbide-a and bacteriopurpurinimide by circular dichroism spectroscopy and its correlation with in vivo photosensitizing efficacy. *Bioorg. Med. Chem. Lett.* **2005**, *15* (13), 3189−3192.

(27) Belgorodsky, B.; Fadeev, L.; Ittah, V.; Benyamini, H.; Zelner, S.; Huppert, D.; Kotlyar, A. B.; Gozin, M. Formation and Characterization of Stable Human Serum Albumin- Tris-malonic Acid [C60] Fullerene Complex. *Bioconjugate Chem.* **2005**, *16* (5), 1058−1062.

(28) Krumkacheva, O. A.; Timofeev, I. O.; Politanskaya, L. V.; Polienko, Y. F.; Tretyakov, E. V.; Rogozhnikova, O. Y.; Trukhin, D. V.; Tormyshev, V. M.; Chubarov, A. S.; Bagryanskaya, E. G.; et al. Triplet Fullerenes as Prospective Spin Labels for Nanoscale Distance Measurements by Pulsed Dipolar EPR Spectroscopy. *Angew. Chem.* **2019**, *131* (38), 13405−13409.

(29) Qu, X.; Komatsu, T.; Sato, T.; Glatter, O.; Horinouchi, H.; Kobayashi, K.; Tsuchida, E. Structure, photophysical property, and cytotoxicity of human serum albumin complexed with tris (dicarboxymethylene)[60] fullerene. *Bioconjugate Chem.* **2008**, *19* (8), 1556−1560.

(30) Gebicki, J. M. Oxidative stress, free radicals and protein peroxides. *Arch. Biochem. Biophys.* **2016**, *595*, 33−39.

(31) Gutteridge, J. Lipid peroxidation and antioxidants as biomarkers of tissue damage. *Clin. Chem.* **1995**, *41* (12), 1819−1828.

(32) Wang, F.; Good, J. A.; Rath, O.; Kaan, H. Y. K.; Sutcliffe, O. B.; Mackay, S. P.; Kozielski, F. Triphenylbutanamines: kinesin spindle protein inhibitors with in vivo antitumor activity. *J. Med. Chem.* **2012**, *55* (4), 1511−1525.

https://dx.doi.org/10.1021/acsbiomaterials.0c00932
ACS Biomater. Sci. Eng. 2020, 6, 5930−5940

(33) Snyder, J. W.; Lambert, J. D.; Ogilby, P. R. 5, 10, 15, 20-Tetrakis (N-Methyl-4-Pyridyl)-21 H, 23H-Porphine (TMPyP) as a Sensitizer for Singlet Oxygen Imaging in Cells: Characterizing the Irradiation-dependent Behavior of TMPyP in a Single Cell. *Photochem. Photobiol.* **2006**, *82* (1), 177−184.
(34) Korytowski, W.; Bachowski, G. J.; Girotti, A. W. Analysis of cholesterol and phospholipid hydroperoxides by high-performance liquid chromatography with mercury drop electrochemical detection. *Anal. Biochem.* **1993**, *213* (1), 111−119.
(35) Michalski, R.; Zielonka, J.; Gapys, E.; Marcinek, A.; Joseph, J.; Kalyanaraman, B. Real-time measurements of amino acid and protein hydroperoxides using coumarin boronic acid. *J. Biol. Chem.* **2014**, *289* (32), 22536−22553.
(36) Sies, H. Ebselen, a selenoorganic compound as glutathione peroxidase mimic. *Free Radical Biol. Med.* **1993**, *14* (3), 313−323.
(37) Olchawa, M.; Krzysztynska-Kuleta, O.; Duda, M.; Pawlak, A.; Pabisz, P.; Czuba-Pelech, B.; Sarna, T. In vitro phototoxicity of rhodopsin photobleaching products in the retinal pigment epithelium (RPE). *Free Radical Res.* **2019**, *53* (4), 456−471.
(38) Huang, L.-K.; Wang, M.-J. J. Image thresholding by minimizing the measures of fuzziness. *Pattern recognition* **1995**, *28* (1), 41−51.
(39) Sharma, S. K.; Chiang, L. Y.; Hamblin, M. R. Photodynamic therapy with fullerenes in vivo: reality or a dream? *Nanomedicine (London, U. K.)* **2011**, *6* (10), 1813−1825.
(40) Ashcroft, J. M.; Tsyboulski, D. A.; Hartman, K. B.; Zakharian, T. Y.; Marks, J. W.; Weisman, R. B.; Rosenblum, M. G.; Wilson, L. J. Fullerene (C60) immunoconjugates: interaction of water-soluble C60 derivatives with the murine anti-gp240 melanoma antibody. *Chem. Commun.* **2006**, No. 28, 3004−3006.
(41) Lapin, N. A.; Vergara, L. A.; Mackeyev, Y.; Newton, J. M.; Dilliard, S. A.; Wilson, L. J.; Curley, S. A.; Serda, R. E. Biotransport kinetics and intratumoral biodistribution of malonodiserinolamide-derivatized [60] fullerene in a murine model of breast adenocarcinoma. *Int. J. Nanomed.* **2017**, *12*, 8289.
(42) Chen, M.; Zhou, S.; Guo, L.; Wang, L.; Yao, F.; Hu, Y.; Li, H.; Hao, J. Aggregation Behavior and Antioxidant Properties of Amphiphilic Fullerene C60 Derivatives Cofunctionalized with Cationic and Nonionic Hydrophilic Groups. *Langmuir* **2019**, *35* (21), 6939−6949.
(43) Krueger, P. J.; Jan, J. Infrared spectra and the molecular conformations of some aliphatic amines. *Can. J. Chem.* **1970**, *48* (20), 3229−3235.
(44) McKean, D.; Duncan, J.; Batt, L. CH stretching frequencies, bond lengths and dissociation energies. *Spectrochimica Acta Part A: Molecular Spectroscopy* **1973**, *29* (6), 1037−1049.
(45) Socrates, G. *Infrared and Raman Characteristic Group Frequencies: Tables and Charts*; John Wiley & Sons: New York, 2004.
(46) Craig, N. C.; Evans, D. A. Infrared and Raman Spectra of cis- and trans-1,2-Dichloro-1,2-difluoroethylene. *J. Am. Chem. Soc.* **1965**, *87* (19), 4223−4230.
(47) Long, F.; Bakule, R. Keto-Enol Transformation of 1, 2-Cyclohexanedione. II. Acid Catalysis in Strongly Acidic Media 1−3. *J. Am. Chem. Soc.* **1963**, *85* (15), 2313−2318.
(48) Campbell, R.; Gilow, H. *β*-Diketones. III. 1, 2 The Effect of Ring Size and Conjugation on Tautomerism. *J. Am. Chem. Soc.* **1962**, *84* (8), 1440−1443.
(49) Buettner, G. R.; Mason, R. P. Spin-trapping methods for detecting superoxide and hydroxyl free radicals in vitro and in vivo. *Critical reviews of oxidative stress and aging: advances in basic science, diagnostics and intervention* **2002**, *1*, 27−38.
(50) Nonell, S.; Redmond, R. On the determination of quantum yields for singlet molecular oxygen photosensitization. *J. Photochem. Photobiol., B* **1994**, *22* (2), 171−172.
(51) Gimenez, R. E.; Vargova, V.; Rey, V.; Turbay, M. B. E.; Abatedaga, I.; Moran Vieyra, F. E.; Paz Zanini, V. I.; Mecchia Ortiz, J. H.; Katz, N. E.; Ostatna, V.; et al. Interaction of singlet oxygen with bovine serum albumin and the role of the protein nano-compartmentalization. *Free Radical Biol. Med.* **2016**, *94*, 99−109.
(52) Vakrat-Haglili, Y.; Weiner, L.; Brumfeld, V.; Brandis, A.; Salomon, Y.; Mcllroy, B.; Wilson, B. C.; Pawlak, A.; Rozanowska, M.; Sarna, T.; et al. The microenvironment effect on the generation of reactive oxygen species by Pd- bacteriopheophorbide. *J. Am. Chem. Soc.* **2005**, *127* (17), 6487−6497.
(53) Ashur, I.; Goldschmidt, R.; Pinkas, I.; Salomon, Y.; Szewczyk, G.; Sarna, T.; Scherz, A. Photocatalytic generation of oxygen radicals by the water-soluble bacteriochlorophyll derivative WST11, non-covalently bound to serum albumin. *J. Phys. Chem. A* **2009**, *113* (28), 8027−8037.
(54) Leonis, G.; Avramopoulos, A.; Papavasileiou, K. D.; Reis, H.; Steinbrecher, T.; Papadopoulos, M. G. A comprehensive computational study of the interaction between human serum albumin and fullerenes. *J. Phys. Chem. B* **2015**, *119* (48), 14971−14985.
(55) Di Giosia, M.; Bomans, P. H.; Bottoni, A.; Cantelli, A.; Falini, G.; Franchi, P.; Guarracino, G.; Friedrich, H.; Lucarini, M.; Paolucci, F.; et al. Proteins as supramolecular hosts for C 60: a true solution of C 60 in water. *Nanoscale* **2018**, *10* (21), 9908−9916.
(56) Soldà, A.; Cantelli, A.; Di Giosia, M.; Montalti, M.; Zerbetto, F.; Rapino, S.; Calvaresi, M. C 60@ lysozyme: a new photosensitizing agent for photodynamic therapy. *J. Mater. Chem. B* **2017**, *5* (32), 6608−6615.
(57) Raoof, M.; Mackeyev, Y.; Cheney, M. A.; Wilson, L. J.; Curley, S. A. Internalization of C60 fullerenes into cancer cells with accumulation in the nucleus via the nuclear pore complex. *Biomaterials* **2012**, *33* (10), 2952−2960.
(58) Zhao, Z.; Fairchild, P. W. In *Dependence of Light Transmission through Human Skin on Incident Beam Diameter at Different Wavelengths, Laser-Tissue Interaction IX*; International Society for Optics and Photonics: 1998; pp 354−360.

https://dx.doi.org/10.1021/acsbiomaterials.0c00932
ACS Biomater. Sci. Eng. 2020, 6, 5930−5940